Original Research Article

Effects of nuclear interaction corrections and trichrome fragment spectra modelling on dose and linear energy transfer distributions in carbon ion radiotherapy

Alessia Bazani [a], Jacob Brunner [b,c], Stefania Russo [a], Antonio Carlino [c], Daniel Simon Colomar [d], Walter Ikegami Andersson [d], Mario Ciocca [a], Markus Stock [c,e], Piero Fossati [c,e], Ester Orlandi [a,f], Lars Glimelius [d], Silvia Molinelli [a], Barbara Knäusl [b,c,*]

[a] *Clinical Department, CNAO National Center for Oncological Hadrontherapy, Pavia, Italy*
[b] *Department of Radiation Oncology, Medical University of Vienna, Austria*
[c] *MedAustron Ion Therapy Center, Wiener Neustadt, Austria*
[d] *RaySearch Laboratories, Stockholm, Sweden*
[e] *Karl Landsteiner University of Health Sciences, Krems, Austria*
[f] *Department of Clinical, Surgical, Diagnostic and Pediatric Services, University of Pavia, Pavia, Italy*

A B S T R A C T

Background and Purpose: Nuclear interaction correction (NIC) and trichrome fragment spectra modelling improve relative biological effectiveness-weighted dose (D_{RBE}) and dose-averaged linear energy transfer (LET_d) calculation for carbon ions. The effect of those novel approaches on the clinical dose and LET distributions was investigated.
Materials and Methods: The effect of the NIC and trichrome algorithm was assessed, creating single beam plans for a virtual water phantom with standard settings and NIC + trichrome corrections. Reference D_{RBE} and LET_d distributions were simulated using FLUKA version 2021.2.9. Thirty clinically applied scanned carbon ion treatment plans were recalculated applying NIC, trichrome and NIC + trichrome corrections, using the LEM low dose approximation and compared to clinical plans (*base RS*). Four treatment sites were analysed: six prostate adenocarcinoma, ten head and neck, nine locally advanced pancreatic adenocarcinoma and five sacral chordoma. The FLUKA and clinical plans were compared in terms of D_{RBE} deviations for $D_{98\%}$, $D_{50\%}$, $D_{2\%}$ for the clinical target volume (CTV) and $D_{50\%}$ in ring-like dose regions retrieved from isodose curves in *base RS* plans. Additionally, region-based median LET_d deviations and global gamma parameters were evaluated.
Results: Dose deviations comparing *base RS* and evaluation plans were within ± 1% supported by γ-pass rates over 97% for all cases. No significant LET_d deviations were reported in the CTV, but significant median LET_d deviations were up to 80% for very low dose regions.
Conclusion: Our results showed improved accuracy of the predicted D_{RBE} and LET_d. Considering clinically relevant constraints, no significant modifications of clinical protocols are expected with the introduction of NIC + trichrome.

1. Introduction

The advantages of carbon ion radiotherapy (CIRT) lie in its physical and radiobiological properties. Compared to photon and proton beams, carbon ions exhibit a sharper lateral penumbra and a steeper distal fall-off, as well as higher linear energy transfer (LET) and increased relative biological effectiveness (RBE) near the Bragg peak [1–4]. To fully exploit CIRT properties, treatment planning systems (TPS) for active scanning techniques require accurate physical dose calculation as well as modelling of the biological interactions.

Physical dose calculations in particle therapy employ both Monte Carlo (MC) and analytical algorithms (pencil beam (PB)) in combination with spatial and density information of the treated object [5,6]. Due to their superior accuracy, MC calculations would be preferable but due to

the increased computational power only analytical algorithms are currently available in commercial TPSs for light ions. In a PB algorithm, the dose is computed by convolving Gaussian-modelled lateral fluence by longitudinal integrated depth dose (IDD) curves given in water and scaled for the water equivalent depth of the calculation point [7–10]. In addition to the limitations of the infinite slab approximation, this approach may result in dose calculation errors due to the water non-equivalence of patient tissues, particularly in terms of nuclear interactions, which can be accounted for by considering the ratio of the probability of nuclear interactions in materials compared to water [8,9,11,12].

In terms of RBE-weighted dose (D_{RBE}) calculation, a monochrome model is currently clinically used to characterize radiation quality over the beam's cross-section [13,14]. The monochrome model assumes that, in regards to the computation of D_{RBE} and dose-averaged LET (LET_d), the particle composition of the radiation field produced by a spot is homogeneous across the transversal plane and only dependent on depth resulting in a very high LET_d outside of the field. However, due to the different scattering angles of different nuclear reaction fragments, radiation quality is dependent on the distance from the central beam axis [15–17]. The analytical trichrome model (*trichrome*) for RBE calculations was developed to improve the accuracy of the biological effectiveness calculation of carbon ions [18]. The *trichrome* model was originally integrated for the microdosimetric kinetic model (mMKM), whereas the local effective model (LEM) has so far been used with monochrome [12,14,19–21]. With the *trichrome* model, the particle composition outside of the field only includes lower LET particles of $Z \leq 2$, which better matches the actual particle distribution.

Currently, commercial TPSs available in Europe for scanned CIRT include neither nuclear interaction correction (*NIC*) nor *trichrome* model-based biological dose computation. The current work aims to assess the effects of these two models on D_{RBE} and LET_d distributions.

The accuracy of D_{RBE} and LET_d prediction based on *NIC* and *trichrome* algorithms was validated with basic treatment plans and target geometries benchmarked against FLUKA MC simulations [22–24]. Clinical treatment plans for several anatomical districts were analysed to assess clinically relevant variations from the current standard.

2. Material and methods

2.1. Theoretical background

NIC accounted for the elemental composition of the traversed medium and, by that, modified the physical dose calculation. An attenuation correction factor for IDDs was introduced via a relation between the electronic stopping power ratio ρ_S (i.e. the ratio of the stopping power in a material to that of water) and the nuclear reaction probability ratio ρ_N (i.e. the ratio of a material's probability of nuclear interaction to that of water) [11]. If $\rho_N > \rho_S$ (e.g. in adipose tissue), the correction factor predicted more nuclear reactions, while the opposite happened if $\rho_S > \rho_N$ (e.g. in bone tissue). In the former case, the dose distribution was lower until the Bragg peak due to increased attenuation of primary carbon ions, while the dose in the tail region was higher due to an enlarged fragment production.

The *trichrome* algorithm for biological dose computation was based on a multiple Gaussian description of the fragments' contribution to the dose profile: the first Gaussian component was mainly determined by primary carbon ions; the second and the third components were composed of heavy fragments with atomic number $Z \geq 3$, and light fragments with $Z \leq 2$, respectively. As a result, a greater concentration of carbon ions yielded higher RBE near the central axis, while the opposite happened for regions with a high concentration of light fragments (i.e. far from the central beam axis). Similarly to MKM, the trichrome model was applied to LEM low dose approximation coefficients in mixed radiation fields via the introduction of a radial dependence in the intrinsic LEM parameters [25]. A detailed theoretical description of the theory behind *NIC* and *trichrome* corrections can be found in Inaniwa et al [11,18].

2.2. Reference FLUKA simulations

Single beam plans with a uniform dose of 3 Gy (RBE) to a cubic target of 4 cm side length were optimized with Raystation-V.11B-DTK (Ray-Search Laboratories, Sweden) using standard interaction settings (*base RS*) and employing *NIC* and *trichrome* corrections (*NIC* + *trichrome*). Slabs of different materials and variable thicknesses were interposed between the beam entrance and the target surface, preceded and followed by 1.5 cm of water (Supplementary Figure S1).

To assess the accuracy of the *NIC* + *trichrome* algorithms, reference D_{RBE} and LET_d distributions were simulated using the FLUKA version 2021.2.9. All plans were calculated with a dose grid resolution of 0.3 cm.

The beam was modelled in FLUKA using a user-defined SOURCE routine which samples beam particles from a phase space according to the RayStation beam model. The HADROTHErapy default settings were enabled, and delta-ray production was disabled. Scoring of LET_d, α and sqrt(β) was achieved with a combination of FLUKA's built-in scoring card USRBIN and user-defined COMSCW routines where each energy deposition was weighted with its corresponding quantity. The ion-specific α values, given as a function of energy for each particle species, were taken from pre-computed tables of the chordoma cell type according to LEM I [13]. The reference D_{RBE} was calculated in a separate script using the LEM low-dose approximation [25].

2.3. Clinical dose calculations

Thirty anonymised scanned CIRT plans from patients treated at MedAustron and CNAO (registry trial number GS1-EK-4/350–2015 and CNAO OSS 64 2023) previously optimized with LEM I in Raystation-V.8B (PBv3.0) and 10B (PBv4.2) were imported into Raystation-V.11B-DTK. Keeping the original spot distribution and weights, the final dose was recalculated with the PBv.5.0 carbon ion dose engine (*base RS* plans), using the LEM low dose approximation [25]. Each plan was reproduced three times (evaluation plans), and the dose distributions were recalculated by applying *NIC*, *trichrome* and a combination of both (*NIC* + *trichrome*). Treatment plans from four different sites were analysed: six prostate adenocarcinoma (PCA), ten head and neck (H&N), nine locally advanced pancreatic adenocarcinoma (LAPC) and five sacral chordomas (SC).

2.4. Evaluation and statistics

To examine the effect on healthy/non-target tissues surrounding the clinical target volume (CTV), three ring-like dose regions based on isodose curves calculated in clinical *base RS* plans were considered, i.e. the region between CTV and 90% isodose (iso90), the region between CTV and 40% isodose (iso40) and the region between 40% and 10% isodose (iso10). For FLUKA simulations iso40 was defined as the region between 90% isodose and 40% isodose instead.

For LET_d additional low-dose regions were defined to investigate the highest expected differences, i.e. the volume between 10% and 2% isodoses (iso2) and the volume between 10% and 0.5% isodoses (iso0.5), for FLUKA simulations and clinical plans, respectively. For the FLUKA simulations, the lower dose limit was selected to avoid significant levels of stochastic fluctuations.

For FLUKA simulations, depth D_{RBE} and LET_d distributions in water along the beam axis and D_{RBE} and LET_d profiles in water in the centre of the target were extracted. This was performed among FLUKA, Raystation without *NIC* + *trichrome* (*base RS*) and including *NIC* + *trichrome*.

To analyse the dose to the CTV and the defined ring-like dose regions in the clinical plans, near-minimum D_{RBE} (D_{RBE} to 98% of the volume ($D_{98\%}$)), median dose ($D_{50\%}$) and near-maximum dose ($D_{2\%}$) were collected for all *base RS* and evaluation plans. The percentage dose

deviations (ΔD) between those D_{RBE} values of all three evaluation plans (D_{eval}) concerning *base RS* plans , were analysed and presented as median dose deviation values [interquartile range]. To assess the outcome for the energy deposition patterns, median LET_d values were collected for the CTVs and above-defined ring-like dose regions, i.e. iso90, iso40, iso10 and iso0.5. Percentage LET_d deviations (ΔLET_d) comparing *base RS* to the evaluation plans were only reported for the *NIC + trichrome* combination, which corresponded to the future clinical implementation.

To assess the agreement between the D_{RBE} and LET_d distributions between different dose computation methods (FLUKA and RayStation) and algorithms (*base RS plans* and *NIC + trichrome*), global gamma evaluations were performed [26]. For FLUKA simulations a RayStation codebase using a tailored in-house dose validation framework and for the clinical plans an in-house written Python script, running on the Raystation script framework was used. γ-pass rate criteria of 2%/1 mm and 5%/1 mm were applied for the FLUKA simulations and of 1%/1 mm for the clinical plans. Mean γ-pass rate values will be reported with the respective standard deviation (SD).

For all dose-volume histogram (DVH) and LET-volume histogram (LVH) criteria reported above, the non-parametric Wilcoxon signed-rank test was applied. The statistical significance of D_{RBE} (comparing *NIC*, *trichrome* and *NIC + trichrome* plans to *base RS* plans) and LET_d deviations (comparing only *NIC + trichrome* to *base RS* plans) was assessed with a significance level of $p < 0.02$ and $p < 0.05$, respectively, pooling all treatment sites together.

3. Results

3.1. FLUKA reference simulations

Fig. 1 shows the comparison of D_{RBE} and LET_d distributions in bone along the beam axis among FLUKA, *base RS* and *NIC + trichrome* underlining a sharp LET_d peak at the distal edge of the target that was not fully modelled in Raystation applying *NIC + trichrome* corrections. The LET_d profile in water *(Fig. 1)* visualised the trichrome effect, where the monochrome approximation assumed a homogeneous particle composition in the transversal plane, which in reality was dominated by protons with low LET. Percentage deviations in median D_{RBE} and median LET_d between *base RS*, *NIC + trichrome* and the reference FLUKA calculations are reported in Supplementary Table S1.

The gamma evaluation comparing dose distributions in RayStation and FLUKA with 5%/1mm criterion showed a very good agreement between both, *base RS* and *NIC + trichrome* and FLUKA calculations (Table 1). γ-passing rates with 2%-1mm criterion in the water showed small deviations (passing rate around or higher than 99%) for adipose and bone cases and larger deviations for the lung and titanium cases (around 97% passing rate, down to 83% for titanium in the iso10 region). *NIC + trichrome* overall improved the γ-passing rate compared to *base RS*, except in the lung case.

The gamma evaluation for LET_d distributions with 2%/1mm criterion showed an improved γ-passing rate in all materials and dose regions when using *NIC + trichrome*, except in the iso2 region in the water and adipose cases (Table 1). The results with γ-pass criteria 5%/1mm at the iso2 dose region showed large deviations when comparing *base RS* to
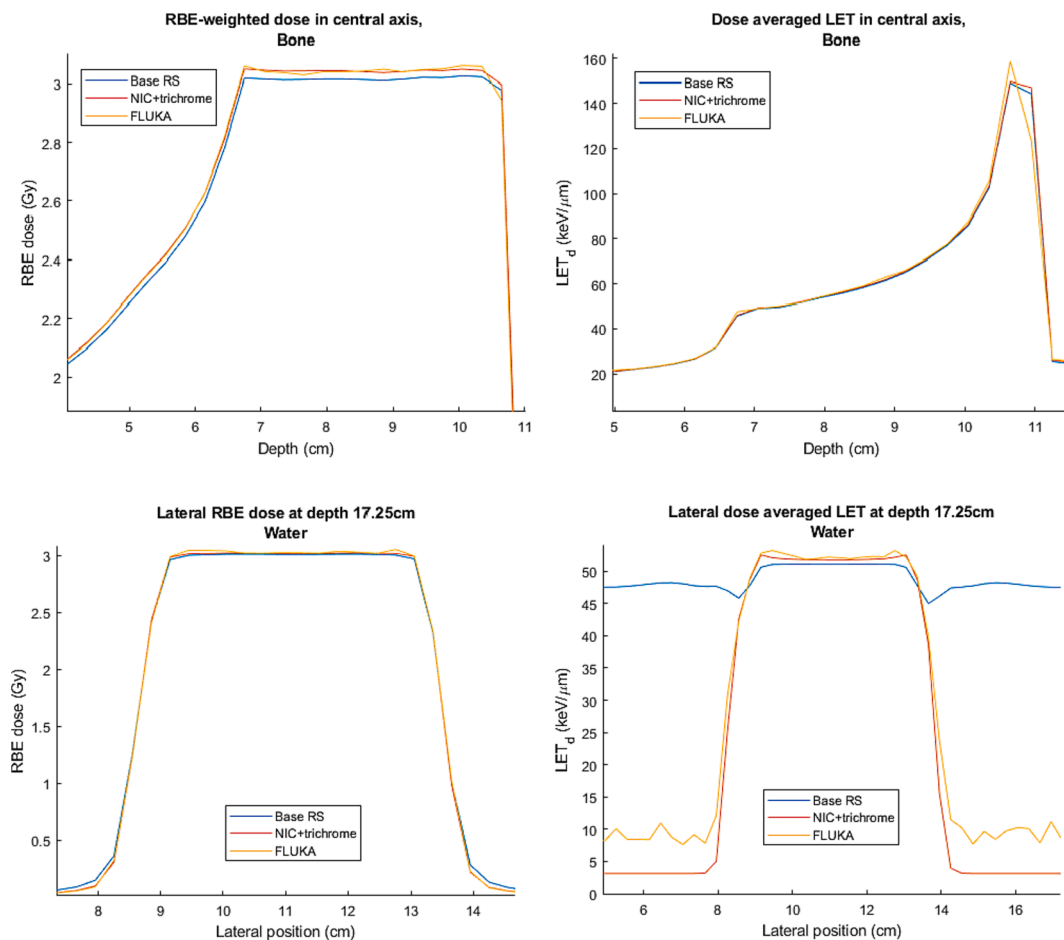

Fig. 1. top) Depth D_{RBE} and LET_d distributions in bone along the beam axis, around the target depth.   bottom) Lateral D_{RBE} and LET_d profiles in water in the centre of the target; Blue line: RayStation without NIC+trichrome (base RS). Red line: RayStation with NIC+trichrome. Yellow line: FLUKA.

Table 1
Global γ-pass rates of the D_{RBE} and LET_d computed in RayStation with (*NIC + trichrome*) and without (*base RS*), with D_{RBE} computed in FLUKA as the reference. Data is presented for each one of the plans with different slab materials, for both 2%/1mm and 5%/1mm criteria and for each of the dose regions.

D_{RBE}		2%/1mm γ-pass rate [%]				5%/1mm γ-pass rate [%]			
Material	Algorithm	Target	iso40	iso10		Target	iso40	iso10	
Water	base RS	98.9	100.0	99.6		100.0	100.0	100.0	
	NIC + trichrome	99.9	99.9	99.8		100.0	100.0	100.0	
Lung	base RS	97.3	99.0	99.6		100.0	100.0	100.0	
	NIC + trichrome	96.9	99.0	98.4		100.0	100.0	100.0	
Adipose	base RS	99.0	97.8	99.8		100.0	100.0	100.0	
	NIC + trichrome	99.7	98.7	99.9		100.0	99.99	100.0	
Bone	base RS	98.0	100.0	99.6		100.0	100.0	100.0	
	NIC + trichrome	99.9	99.9	99.9		100.0	100.0	100.0	
Titanium	base RS	0.0	81.9	59.2		99.1	100.0	100.0	
	NIC + trichrome	97.1	96.1	83.1		100.0	100.0	100.0	

LET_d		2%/1mm γ-pass rate [%]				5%/1mm γ-pass rate [%]			
Material	Algorithm	Target	iso40	iso10	iso2	Target	iso40	iso10	iso2
Water	base RS	96.9	98.2	79.3	75.6	100.0	99.8	94.9	88.9
	NIC + trichrome	97.6	98.4	98.0	68.4	100.0	99.8	100.0	99.5
Lung	base RS	91.4	99.2	76.8	83.6	95.8	99.6	90.4	91.2
	NIC + trichrome	92.8	99.3	91.6	91.6	95.7	99.8	95.7	99.1
Adipose	base RS	96.4	99.4	79.0	73.7	100.0	100.0	97.9	77.7
	NIC + trichrome	98.5	99.6	97.3	67.8	100.0	100.0	99.8	99.6
Bone	base RS	89.5	97.6	75.0	86.6	92.9	98.8	85.0	92.6
	NIC + trichrome	92.5	98.3	91.9	90.8	92.9	98.8	94.0	99.3
Titanium	base RS	90.4	93.5	80.7	89.2	100.0	95.6	89.4	94.6
	NIC + trichrome	99.9	95.6	97.8	96.4	100.0	95.6	99.2	99.7

FLUKA, whereas the γ-passing rates for all cases were higher than 99% when using *NIC + trichrome*. For the target and the iso40 regions, the LET_d γ-passing rates with 5%/1mm criterion were comparable for *base RS* and *NIC + trichrome*, but some of them had a significant number of fails (around 5% fail rate or higher).

3.2. Clinical dose calculations

The introduction of *NIC* led to a median reduction of $D_{50\%}$ below 1% in the CTV, iso90 and iso40, for all considered treatment plans. A sign variation was reported only for sacral chordomas (increase by median 0.9% [interquartile range 0.7%]) in the lower dose region (iso10). *Trichrome* modelling resulted in a median dose increase of $D_{98\%}$, $D_{50\%}$ and $D_{2\%}$ in the CTV; the trend was variable for iso10 depending on the treatment site, where negative variations of $D_{50\%}$ up to −0.9% [0.2%] for sacral chordomas cases were observed. $\Delta D_{50\%}$ never exceeded $\pm 1\%$. The median ΔD values for each indication for all three evaluation doses are reported in Supplementary Table S2. A D_{RBE} and LET_d comparison is exemplified for a prostate patient in Fig. 2.

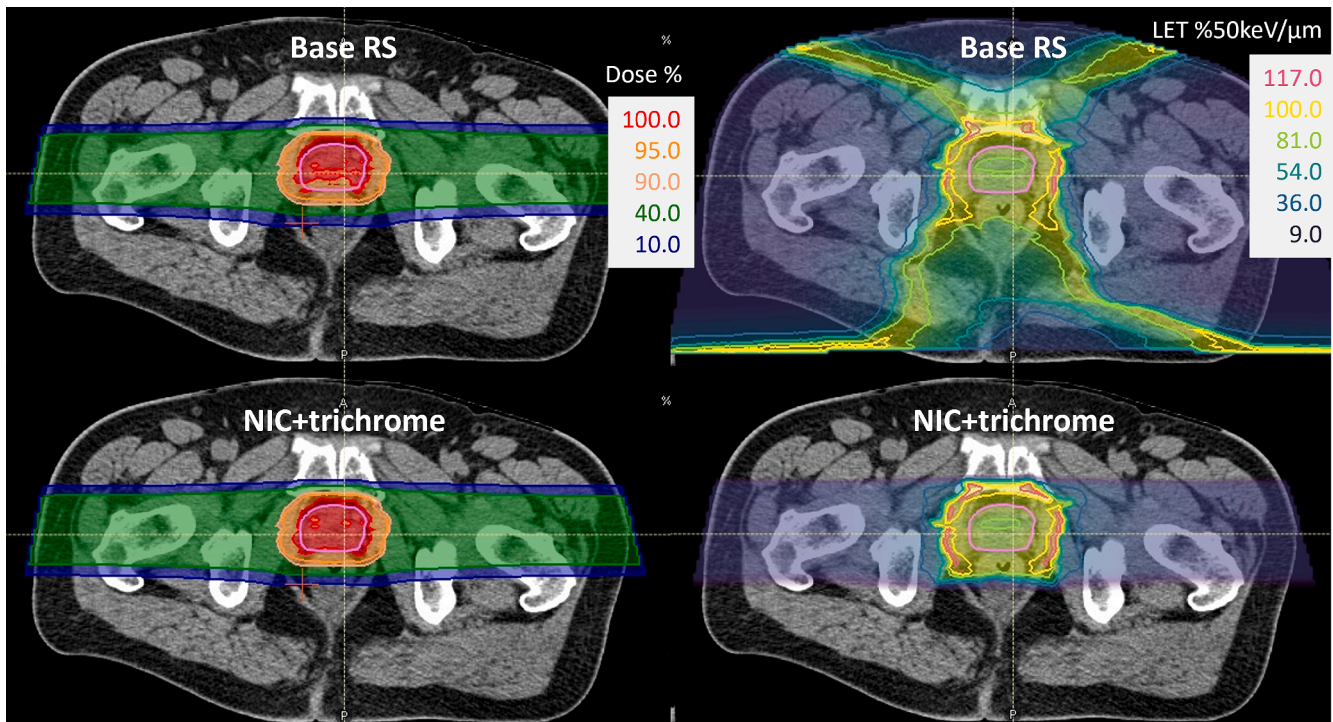The combination of *NIC + trichrome* led to overall smaller dose

Fig. 2. Base RS vs NIC+trichrome plan for a prostate adenocarcinoma case; left) D_{RBE} distribution right): LET_d distributions.

deviations compared to the evaluation of the *NIC* and *tri-chrome* alone with a median increase < 0.5%. This trend was observed in all the analysed dose regions, except iso10 in H&N where $\Delta D_{50\%}$ was -0.8% [0.7]. Fig. 3 shows box plots of the median ΔD values and interquartile ranges comparing *NIC + trichrome* to *base RS* plans for the CTV (D$_{98\%}$, D$_{50\%}$ and D$_{2\%}$) and the ring-like dose regions (D$_{50\%}$) for the different anatomical districts. Dose deviations comparing *base RS* and evaluation plans were not statistically significant for any dose/volume metrics that were considered ($p > 0.02$). The mean γ-pass rate restricted to CTV and ring-like dose regions was > 97% for all *NIC + trichrome* plans averaged over all patients within an anatomical district (Table 2).

When considering the CTV, the LET$_d$ analysis showed deviations $\leq$ 1% comparing *base RS* and *NIC + trichrome* plans for all treatment sites, except prostate adenocarcinoma (median $\Delta LET_d > 1\%$ (1.71 [1.81]%)). Considering the different treatment sites, the trend of a ΔLET_d increase/decrease was consistent for the iso90 and iso0.5 rings. For the iso40 and iso10, the median ΔLET_d showed an increase for the PCA cases, while the other anatomical districts exhibited a median ΔLET_d decrease. The most relevant variations in LET$_d$ distribution were observed in iso0.5, where a statistically significant negative median deviation of up to 80% was reported for PCA and LAPC cases ($p < 0.05$). The corresponding box plots comparing ΔLET_d values between *base RS* and *NIC + trichrome* plans are illustrated in Fig. 4.

4. Discussion

The effect of nuclear interaction correction and trichrome modelling on carbon ion dose and LET$_d$ distributions was validated and compared against reference FLUKA MC simulations. Investigations in a phantom geometry and analysing 30 clinical treatment plans for various anatomical districts revealed that enhancing PB modelling did not affect the clinical dose distributions, while LET$_d$ prediction was significantly improved.

For the phantom geometries, an improved agreement of the PB algorithm with FLUKA reference simulations was observed for the LET$_d$ calculations when applying *NIC + trichrome* instead of monochrome (*base RS*). One exception was found for calculations in the iso2 region with the 2%/1mm criteria in pure water and adipose tissue where *NIC* had no impact [11,12]. Especially in the low dose region, (iso2 and iso10) comprising the lateral fall-off and the tail region, *NIC + trichrome*

Table 2
Average γ-pass rates (1%/1mm criteria) and standard deviations (SD) restricted to the CTV and the defined ring-like dose regions comparing *base RS* plans with the *NIC + trichrome* plans; the values were averaged over anatomical district defining the standard deviation (SD).

γ-pass rates (1%/1mm) [%] (SD)				
	PCA	*H&N*	*LAPC*	*SC*
CTV	100.0 (0.1)	99.7 (0.9)	100.0 (0.0)	100.0 (0.0)
Iso-90%	100.0 (0.1)	99.9 (0.0)	100.0 (0.0)	100.0 (0.3)
Iso-40%	99.8 (0.1)	100.0 (0.1)	100.0 (0.0)	100.0 (0.0)
Iso-10%	97.1 (1.6)	100.0 (0.5)	99.5 (0.1)	99.9 (0.1)

outperformed monochrome achieving γ-pass rates of 99% for almost all tissue slabs for the 5%/1mm criteria. Even though LET$_d$ values in low-dose regions far away from the target might not be clinically relevant, actual high LET$_d$ regions are more easily discerned. For lung and bone, the LET$_d$ γ-pass rates in the target region were lower than for the rest of the materials with only a slight improvement by the introduction of *NIC* and *trichrome*. In these cases, the RayStation PB algorithm did not capture the sharpness of the distal LET$_d$ peak (Fig. 1), which was unaffected by *trichrome*.

D$_{RBE}$ calculation could be improved by employing *NIC + trichrome* for all tissue material slabs and dose regions except for the target region with lung material in the beam path. For the elemental composition of the lung, the *NIC* algorithm had a negligible effect because ρ_S nearly equals ρ_N [11,12]. The slightly worse γ-pass rate for *NIC + trichrome* for the 2%/1mm criteria resulted from the fact that lower physical dose and higher RBE factor predicted in FLUKA averaged out in *base RS*. In the remaining cases (adipose, bone and titanium slabs), both *NIC* and *trichrome* played a significant role resulting in moderately improved D$_{RBE}$ and LET$_d$ passing rates in the target region for adipose and bone to dramatically increase γ-pass rates for titanium in all dose regions. The largest improvements in D$_{RBE}$ were observed in the bone and titanium cases since the effects of both *NIC* and *trichrome* contributed to an increase of the dose inside the target and a decrease in the dose outside, which was not well predicted with *base RS* [11,12,18].

For the clinical cases, the introduction of *NIC* and *trichrome* in the PB dose calculation algorithm did not affect the clinical acceptability, as all DVH parameter deviations (D$_{98\%}$, D$_{50\%}$ and D$_{2\%}$) were considered
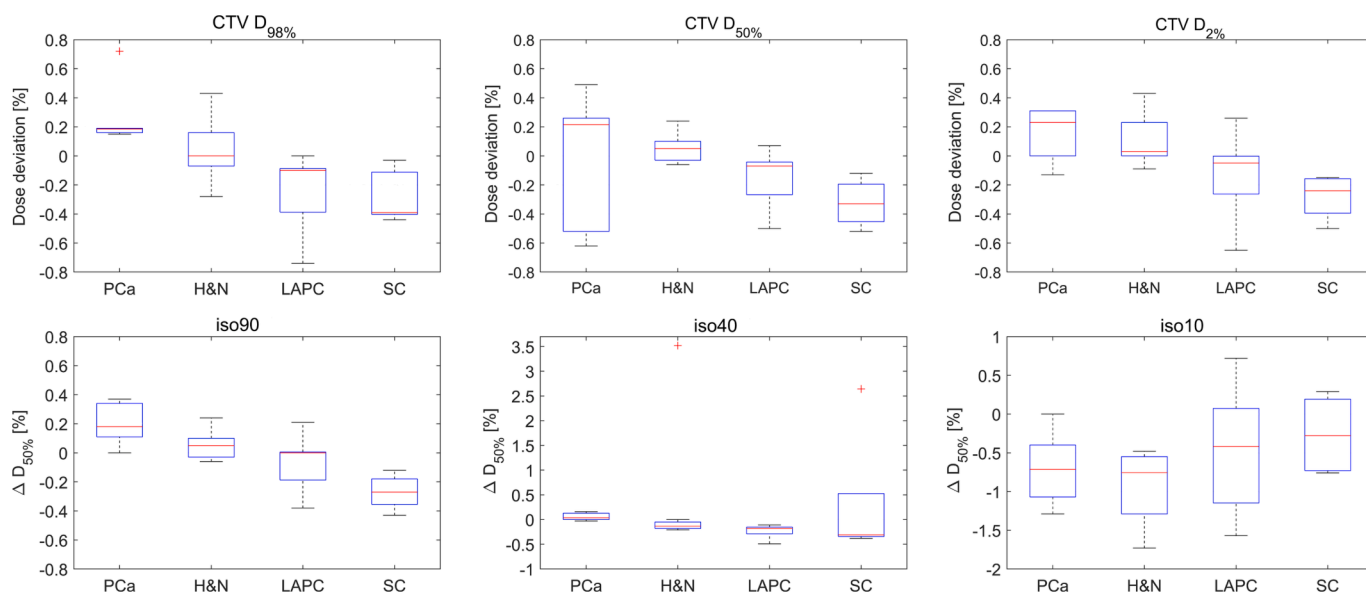

Fig. 3. Percentage median dose deviations and interquartile ranges comparing *base RS* and *NIC+trichrome* plans. D$_{98\%}$, D$_{50\%}$ and D$_{2\%}$ (upper part) for the CTV and D$_{50\%}$ for iso90, iso40 and iso10 (lower part) are plotted in the different diagrams. All plans included in this boxplot were recalculated with *NIC+trichrome* and plotted for each anatomical district separately. The boxplots show the median and 25th to 75th percentile, with the whiskers displaying 1.5 times inter-quartile range.
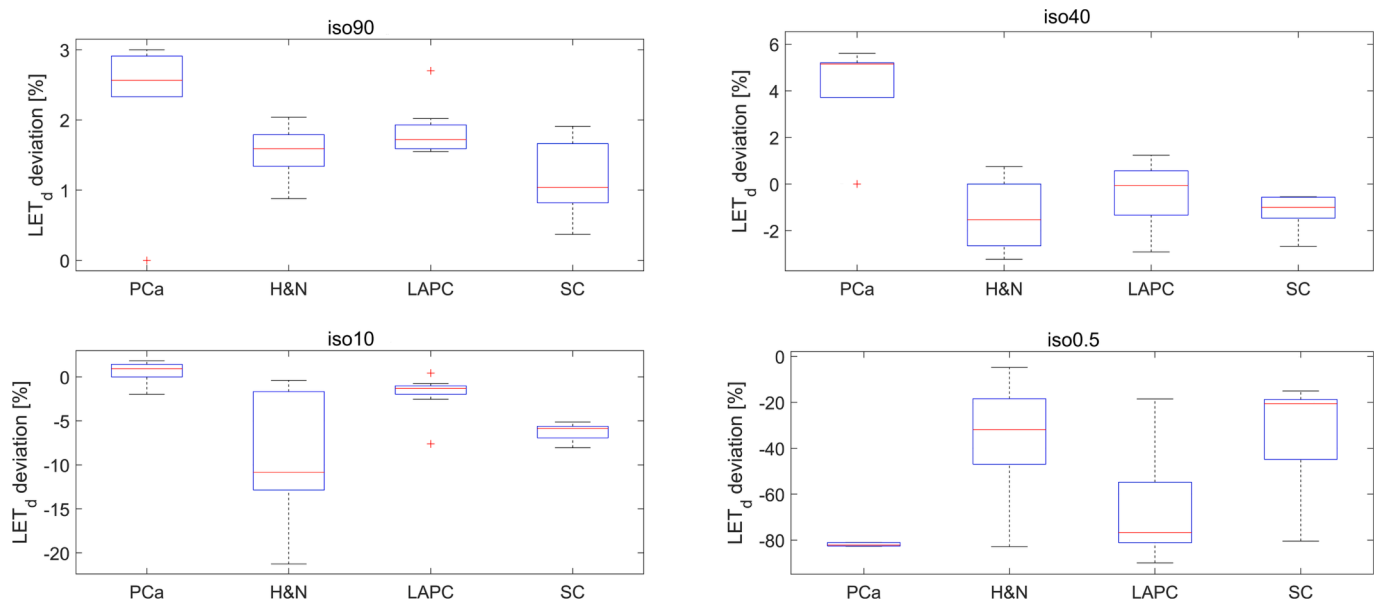
Fig. 4. Percentage median LET_d deviations and interquartile ranges in ring-like dose regions, namely iso90, iso40, iso10 and iso0.5, comparing *base RS* and *NIC+trichrome* plans stratified by anatomical districts analysed. The boxplots show the median and 25th to 75th percentile, with the whiskers displaying 1.5 times inter-quartile range.

negligible and were not statistically significant. This was further confirmed by the excellent γ-pass rate (1%/1mm) with a median value larger than 99% in the target region and surrounding dose regions.

Nuclear interaction correction alone accounted for the water-non-equivalence of the irradiated tissues [27]. The cross-section adjustment decreased the physical dose inside the target as the additional elastic scatter of the primary ions was accounted for and resulted in a minor median decrease (<1%) of $D_{50\%}$ in the target region for all anatomical districts. Adding solely *trichrome* stratified the incident particles into three halos, with the dominating particles being primary ions in the centre and light ion fragments in the lateral periphery [18]. Also, this change in particle type and LET_d resulted in a minor median increase (<1%) of $D_{50\%}$ in the target region. The observed deviations in the clinical plans confirm the previous non-clinical examinations in the frame of the algorithm development and phantom studies [28].

Notable changes between the LET_d *NIC + trichrome* and *base RS* plans were observed, particularly in regions far from the central beam axis (iso0.5). With little contribution from the primary ions, light fragments dominated the energy deposition, which drastically lowered the LET_d in the edge-of-field regions. With increasing ion energies e.g. in PCA and LAPC cases, the lateral fall-off of LET_d increased compared to the monochrome approximation [13,14,18]. Thus, reported differences grew more pronounced, compared to shallower targets in H&N and SC cases. *NIC* altered the physical dose, which caused LET_d changes, while *NIC + trichrome* scaled the halos according to the particle spectra assigned by *trichrome*. All studies investigating the association between LET_d and clinical outcomes in carbon ion radiotherapy will benefit from a more accurate calculation of the clinical LET_d distribution.

In conclusion, the results showed a general improvement in the accuracy of the predicted RBE-weighted dose and LET_d. Considering clinically relevant goals and constraints, no significant modifications of clinical protocols are expected with the introduction of *NIC* and *trichrome*.

Declaration of competing interest

The authors declare the following financial interests/personal relationships which may be considered as potential competing interests: Lars Glimelius, Daniel Simon Colomar, Walter Ikegami Andersson

Appendix A. Supplementary data

Supplementary data to this article can be found online at https://doi.org/10.1016/j.phro.2024.100553.

References

[1] Durante M, Paganetti H. Nuclear physics in particle therapy: a review. Rep Prog Phys 2016;79:096702. https://doi.org/10.1088/0034-4885/79/9/096702.

[2] Kinsella TJ, Pacelli R, Durante M, Trifiletti DM, Malouff TD, Mahajan A, et al. Carbon ion therapy: a modern review of an emerging technology. Front Oncol 2020;10:82. https://doi.org/10.3389/fonc.2020.00082.

[3] Rackwitz T, Debus J. Clinical applications of proton and carbon ion therapy. Semin Oncol 2019;46:226–32. https://doi.org/10.1053/J.SEMINONCOL.2019.07.005.

[4] Suit H, DeLaney T, Goldberg S, Paganetti H, Clasie B, Gerweck L, et al. Proton vs carbon ion beams in the definitive radiation treatment of cancer patients. Radiother Oncol 2010;95:3–22. https://doi.org/10.1016/J.RADONC.2010.01.015.

[5] Hollmark M, Belkić D, Gudowska I, Brahme A. Influence of multiple scattering and energy loss straggling on the absorbed dose distributions of therapeutic light ion beams: I. Analytical pencil beam model. Phys Med Biol 2004;49:3247. https://doi.org/10.1088/0031-9155/49/14/016.

[6] Parodi K, Mairani A, Sommerer F. Monte Carlo-based parametrization of the lateral dose spread for clinical treatment planning of scanned proton and carbon ion beams. J Radiat Res 2013;54:i91. https://doi.org/10.1093/JRR/RRT051.

[7] Kanematsu N. Semi-empirical formulation of multiple scattering for the Gaussian beam model of heavy charged particles stopping in tissue-like matter. Phys Med Biol 2009;54:N67. https://doi.org/10.1088/0031-9155/54/5/N01.

[8] Kanematsu N, Inaniwa T, Koba Y. Relationship between electron density and effective densities of body tissues for stopping, scattering, and nuclear interactions of proton and ion beams. Med Phys 2012;39:1016–29. https://doi.org/10.1118/1.3679339.

[9] Al-Sulaiti L, Shipley D, Thomas R, Owen P, Kacperek A, Regan PH, et al. Water equivalence of some plastic-water phantom materials for clinical proton beam

dosimetry. Appl Radiat Isot 2012;70:1052–7. https://doi.org/10.1016/J.APRADISO.2012.02.002.

[10] Moyers MF, Vatnitsky AS, Vatnitsky SM. Factors for converting dose measured in polystyrene phantoms to dose reported in water phantoms for incident proton beams. Med Phys 2011;38:5799–806. https://doi.org/10.1118/1.3639119.

[11] Inaniwa T, Kanematsu N, Hara Y, Furukawa T. Nuclear-interaction correction of integrated depth dose in carbon-ion radiotherapy treatment planning. Phys Med Biol 2014;60:421. https://doi.org/10.1088/0031-9155/60/1/421.

[12] Inaniwa T, Kanematsu N, Tsuji H, Kamada T. Influence of nuclear interactions in body tissues on tumor dose in carbon-ion radiotherapy. Med Phys 2015;42:7132–7. https://doi.org/10.1118/1.4936105.

[13] Kramer M, Scholz M. Treatment planning for heavy-ion radiotherapy: calculation andoptimization of biologically effective dose. Phys Med Biol 2000;45:3319. https://doi.org/10.1088/0031-9155/45/11/314.

[14] Inaniwa T, Furukawa T, Kase Y, Matsufuji N, Toshito T, Matsumoto Y, et al. Treatment planning for a scanned carbon beam with a modified microdosimetric kinetic model. Phys Med Biol 2010;55:6721. https://doi.org/10.1088/0031-9155/55/22/008.

[15] Inaniwa T, Furukawa T, Matsufuji N, Kohno T, Sato S, Noda K, et al. Clinical ion beams: semi-analytical calculation of their quality. Phys Med Biol 2007;52:7261. https://doi.org/10.1088/0031-9155/52/24/005.

[16] Matsufuji N, Komori M, Sasaki H, Akiu K, Ogawa M, Fukumura A, et al. Spatial fragment distribution from a therapeutic pencil-like carbon beam in water. Phys Med Biol 2005;50:3393. https://doi.org/10.1088/0031-9155/50/14/014.

[17] Nose H, Kase Y, Matsufuji N, Kanai T. Field size effect of radiation quality in carbon therapy using passive method. Med Phys 2009;36:870–5. https://doi.org/10.1118/1.3077490.

[18] Inaniwa T, Kanematsu N. A trichrome beam model for biological dose calculation in scanned carbon-ion radiotherapy treatment planning. Phys Med Biol 2014;60:437. https://doi.org/10.1088/0031-9155/60/1/437.

[19] Hawkins RB. A microdosimetric-kinetic model of cell death from exposure to ionizing radiation of any LET, with experimental and clinical applications. Int J Radiat Biol 2009;69:739–55. https://doi.org/10.1080/095530096145481.

[20] Scholz M, Kraft G. Track structure and the calculation of biological effects of heavy charged particles. Adv Sp Res 1996;18:5–14. https://doi.org/10.1016/0273-1177(95)00784-C.

[21] Scholz M, Kraft G. The physical and radiobiological basis of the local effect model: a response to the commentary by R. Katz Radiat Res 2004;161:612–20. https://doi.org/10.1667/RR3174.

[22] Linear S, Ferrari A, Sala PR, Fasso A, Ranft J. FLUKA: A Multi-Particle Transport Code 2005.

[23] Battistoni G, Bauer J, Boehlen T, Cerutti F, Chin M, Dos Santos AR, et al. The FLUKA code: an accurate simulation tool for particle therapy. Front Oncol 2016;6:116. https://doi.org/10.3389/fonc.2016.00116.

[24] Böhlen TT, Cerutti F, Chin MPW, Fassò A, Ferrari A, Ortega PG, et al. The FLUKA code: developments and challenges for high energy and medical applications. Nucl Data Sheets 2014;120:211–4. https://doi.org/10.1016/J.NDS.2014.07.049.

[25] Krämer M, Scholz M. Rapid calculation of biological effects in ion radiotherapy. Phys Med Biol 2006;51:1959. https://doi.org/10.1088/0031-9155/51/8/001.

[26] Low DA, Harms WB, Mutic S, Purdy JA. A technique for the quantitative evaluation of dose distributions. Med Phys 1998;25:656–61. https://doi.org/10.1118/1.598248.

[27] Lühr A, Hansen DC, Teiwes R, Sobolevsky N, Jäkel O, Bassler N. The impact of modeling nuclear fragmentation on delivered dose and radiobiology in ion therapy. Phys Med Biol 2012;57:5169. https://doi.org/10.1088/0031-9155/57/16/5169.

[28] Schafasand M, Resch AF, Traneus E, Glimelius L, Fossati P, Stock M, et al. Technical note: In silico benchmarking of the linear energy transfer-based functionalities for carbon ion beams in a commercial treatment planning system. Med Phys 2023;50:1871–8. https://doi.org/10.1002/MP.16174.